Pergamon

Cement and Concrete Research, Vol. 28, No. 12, pp. 1695–1705, 1998

0008-8846/98 $–see front matter

PII S0008-8846(98)00159-8

IMAGE-BASED CHARACTERIZATION OF CEMENT PORE STRUCTURE USING WOOD'S METAL INTRUSION

Kelly L. Willis, Anne B. Abell, and David A. Lange[1]
Department of Civil Engineering, University of Illinois, Urbana, IL 61801, USA

(Received July 1, 1997; in final form September 4, 1998)

ABSTRACT

Mercury intrusion porosimetry is a widely used technique for characterization of the pore size distribution of cement-based materials. However, the technique has several limitations, among which are the ink bottle effect and a cylindrical pore geometry assumption that lead to inaccurate pore size distribution curves. By substituting Wood's metal for mercury as the intruding liquid, scanning electron microscopy and imaging techniques can be applied to the sample after intrusion. The molten Wood's metal solidifies within the pore structure of the sample, which allows it to be sectioned and observed in the scanning electron microscopy. From here, the sample can be analyzed both qualitatively, by observing the changes in the appearance of the sample as the intrusion process progresses, and quantitatively, by applying image analysis techniques. This study provides insight for better interpretation of mercury intrusion porosimetry results and the possibility for quantitative characterization of the spatial geometry of pores in cement-based materials. © *1998 Elsevier Science Ltd*

Introduction

The significance of porosity has been understood by researchers involved in the study of cement and concrete for six decades. In 1936, T.C. Powers and the Portland Cement Association began groundbreaking work that aimed to relate cement chemistry and concrete technology. In 1947 this work led Powers and Brownyard (1) to establish the importance of the porosity of cement paste by developing a direct relationship between porosity and strength.

As the understanding that porosity has a direct effect on properties like strength, fracture energy, toughness, elastic properties, permeability, and durability became more well known, researchers began to seek methods to characterize the pore structure of cement and concrete. Many methods were developed, including small angle x-ray scattering and Brunauer-Emmitt-Teller (BET) adsorption. However, the most predominant method used is mercury intrusion porosimetry (MIP). This method is easy to perform and capable of spanning a large range of pore sizes but is limited in its application because of the errors associated with the method.

MIP forces mercury into the pores of a material by gradually increasing pressure. At each

[1]To whom correspondence should be addressed.

discrete pressure increment, the volume of mercury intruded into the pores is recorded. This information can then be converted into volume of porosity and pore size distribution. The translation of intruding pressure to pore size is given by the Washburn equation (2):

$$P = \frac{-4\gamma \cos \theta}{d}$$

where γ is the surface energy of the liquid, θ is the contact angle between the liquid and the pore walls, and d is the diameter of the intruded pore.

MIP has been used to characterize almost every variation of cement paste and concrete. It has been used to examine the interfacial transition zone (3), the influence of water-to-cement ratio on paste (4), the effects of admixtures (5), the detection of cracks (6), and the relation between porosity and permeability (7). It is an invaluable tool for comparing the pore structure of different types of cement-based materials.

However, the method has many limitations. First, the Washburn equation was derived based on the assumption that the pores intruded are cylindrical. A second problem is known as the "ink bottle" effect, in which a larger pore is preceded in the intrusion path of the mercury by a smaller neck. This problem produces pore size distribution curves with erroneously high volumes of smaller pores and erroneously small volumes of larger pores. The proper assumption to use for the contact angle has also been researched and debated (8,9). An error in the contact angle assumption that differs from the true value by 1° can result in an error of 2%. Another problem lies in the fact that the sample must be dried prior to intrusion. It has been well documented that some microstructural damage occurs during the drying process. Another possibility for microstructural damage occurs upon intrusion. Feldman (10) found that at pressures above 70 MPa, the mercury breaks down fragile walls within the cement microstructure. However, he noted this only in extremely low porosity pastes. In recent work by Olson et al. (11), microstructural damage was found in a 6-month-old sample of ordinary Portland cement paste by observing postintrusion samples in an environmental scanning electron microscope (SEM).

A technique that employs the principles of MIP but is capable of utilizing modern microscopy techniques to eliminate some of the errors associated with MIP was used to characterize the porosity of sandstones (12,13). This technique was dubbed "Wood's metal intrusion porosimetry" (WMIP). Dullien and Dhawan (13) employed the principles of quantitative stereology to relate the two-dimensional sections they obtained using the SEM to the size distribution of the three-dimensional pore network.

Wood's metal intrusion has been applied to concrete by Scrivener and Nemati (14) in an exploration of the cement paste/aggregate interfacial zone. Chang et al. (15) applied the method in a study of cracks in marble structures as they exist under load and developed a crack propagation model.

It is the purpose of this study to apply WMIP to mortars to study the sequence of intrusion and explore the misrepresentation of size in MIP data. The results will also enable a qualitative understanding of the mechanisms and processes occurring during the intrusion process.

Experimental

In this experiment two mortars of different water-to-cement (w/c) ratios were used to investigate the pore structure as characterized by Wood's metal intrusion. The properties of

TABLE 1
Properties of mortars tested.

	Fresh air content (%)	Bulk specific gravity	Total porosity by oven drying at 14 days (%)	14-day strength (psi)
0.4 W/C	8	2.30	16	4800
0.6 W/C	4	2.20	23	3000

the fresh and hardened mortar were measured, both mercury intrusion and Wood's metal intrusion were performed, and the Wood's metal intruded samples were sectioned and imaged using a SEM. The resulting images were then further examined using image analysis techniques.

Materials

Two mortars of ordinary Portland cement with w/c ratios of 0.4 and 0.6 with a 1:2 ratio by weight of cement to ASTM 20/30 silica sand were tested. The mortars were mixed in a Hobart paddle mixer for 1 min dry and an additional 2 min after adding the water. The fresh air content of the two mortars was determined using ASTM C185 and was found to be 8% and 4% for the 0.4 and 0.6 w/c mixes, respectively. The mortars were cast in 1-inch by 1.5-inch by 7-inch Plexiglas prisms. They were vibrated and rodded to ensure proper compaction, cured for 24 h, demolded and further cured at 100% relative humidity for 14 days. The material properties of the 14-day-old mortars are given in Table 1.

Procedure

Wood's metal. The Wood's metal used in this experiment was acquired from Alfa Aesar Co. and had a chemical composition of 50% bismuth, 26.7% lead, 13.3% tin, and 10% cadmium by weight. The material has a freezing point of 65.5°C, a specific gravity of 9.7 g/cm^3, and is insoluble in water. There is no specific value listed for the volume change of the alloy on crystallization. However, a value for a similar alloy was found to be 0.0057 mm/mm expansion 500 h after casting (16). The contact angle for Wood's metal in contact with mortar was confirmed by video microscopy to be 130°, a value commonly used in MIP.

The intrusion process

The experimental set-up used to intrude Wood's metal into the samples was composed of a high-pressure nitrogen gas tank (maximum pressure: 6000 psi), a mechanical vacuum pump and gauge, and an autoclave. The hose and valves were constructed such that both the pressure and vacuum could be applied separately to the pressure vessel through a single hose line. A schematic of the equipment is shown in Figure 1.

The samples were prepared for the high-pressure autoclave by coring the mortar bars into 3/8-inch diameter cylinders and using a low-speed diamond saw to remove the cast ends.

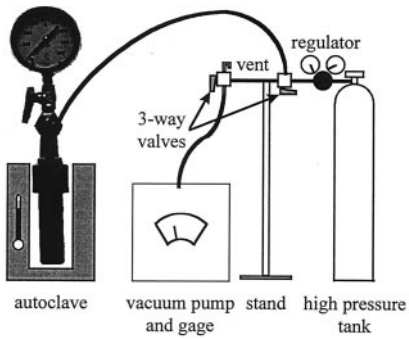

FIG. 1.
Schematic diagram of Wood's metal intrusion apparatus.

These samples were oven dried at 105°C for at least 24 h. The sample was then inserted into a glass test tube with small chunks of the solidified Wood's metal. A short steel rod was added to the test tube to serve as a weight to keep the sample submerged in the molten Wood's metal.

The test tubes were then loaded into the pressure vessel and evacuated to 50 μm (the same vacuum pressure that is used in the mercury intrusion porosimeter used in this work). After the vacuum was attained the vessel was heated to 100°C to ensure that the metal was fully molten. This increase in temperature usually resulted in a slight rise in the vacuum, so after heating the sample was evacuated until it stabilized at 50 μm. Once the vacuum had stabilized the vessel was vented and gradual pressure applied until the pressure for that experimental run was reached. The pressures used to intrude the molten metal into five samples of each mortar specimen were 500, 1000, 1500, 3000, and 5000 psi. The sample remained under pressure and at temperature for 15 min in order to ensure that the metal had sufficient time to intrude. The vessel inlet valve was then closed off, the heat was turned off, and the vessel was allowed to cool to room temperature with the desired pressure still in the chamber.

Sample preparation

The sample, encased in solidified Wood's metal, was removed from the test tube. The cylindrically shaped sample was sectioned with a low-speed diamond saw to yield three surfaces for each sample for microscopic study. The three surfaces were vacuum impregnated with a low-viscosity, low-temperature cure epoxy (Epo-Thin, available from Buehler), and cast within a single epoxy stub. Each stub was 32 mm in height and 1½-inch diameter. A total of ten stubs (five different pressures for two different w/c ratios) with three sections in each stub were cured.

The stubs were ground with a 45-μm diamond wheel and silicon carbide sandpaper grits of 320 and 600. They were then polished using diamond pastes in steps of 6, 3, 1, and 0.05 μm. A Buehler Isomet mechanical polishing machine was used in each of these steps and propylene glycol was used as the lubricant. The samples were cleaned in an ultrasonic bath

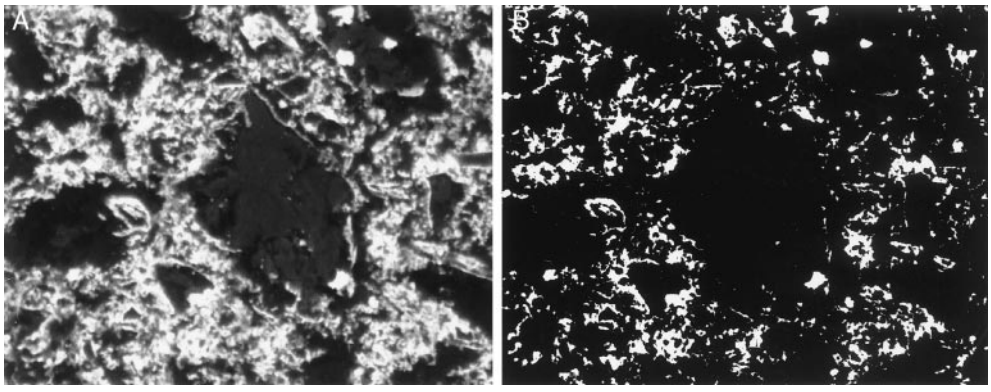

FIG. 2.
Sample images of 0.4 w/c mortar intruded at 5000 psi (magnification 1500× 15 keV) in (*A*) gray scale and (*B*) binary (field width 85 μm; metal is white).

of isopropyl alcohol for 30 s between each step to ensure all contaminants were removed before moving to a finer grit.

Finally, the samples were coated with a very thin (submicron) layer of carbon in a carbon evaporator and were given a stripe of silver paint before mounting on aluminum stubs to provide a good electrical connection, which facilitates high-quality images from the SEM. This step may be redundant for samples fully impregnated with Wood's metal, but all samples regardless of amount of intruded Wood's metal were similarly prepared.

Image analysis

Each of these ten samples were observed in an SEM using backscattered electrons. Sixty images (20 from each of three surfaces) were taken for each sample at a magnification of 1500× and at an SEM voltage of 15 keV. The magnification of 1500× was selected because it was sufficient to resolve capillary pore shapes at the micron scale. Much higher magnifications are hard to use because consistent image quality is difficult to maintain.

After the images were taken and stored they were examined to determine an optimum threshold value that could effectively differentiate between the areas of the image that were metal and those that were mortar matrix. Each sample set of images was then run through a computer software program that thresholded the image, created a binary image, computed the area fraction of the image that was metal, and analyzed the "particles" of metal in the image that identify intruded pore space. Sample images are given in Figure 2. The particle analysis resulted in a listing of the area of each particle and the size of its major and minor axes. All of the image analysis was done using the National Institute of Health's NIH Image, which can be obtained from *http://rsb.info.nih.gov/nih-image/*.

The 60 area fraction values were averaged for each pressure, and statistical analysis was completed. These average values correlate directly to the volume fraction of metal intruded into the sample at that specific pressure. Pore sizes were also measured from binary images of the Wood's metal samples. Calibration of the 1500× image determined the size of a pixel

to be 0.081 μm by 0.081 μm. The image analysis software reported the size (i.e., area) of each contiguous pore, allowing calculation of pore fraction and pore size distribution. Because MIP reported the diameter of the pores, it was convenient to reconcile the units to allow comparison of the two techniques. To represent both the Wood's metal pore data and the MIP data in areal units, the MIP data were converted from pore diameters to pore areas using an assumption of cylindrical pore geometry and a contact angle of 130°. The reader should note that use of areal units inflates the relative differences between techniques as compared to linear units. For example, a 10 times larger pore diameter corresponds to a 100 times larger pore cross-sectional area.

Results and Discussion

Sequence of intrusion

A typical series of backscattered electron images for the 0.6 w/c sample at each pressure is presented in Figure 3. Figure 3A shows infiltration at 500 psi, the lowest pressure analyzed. It shows metal in the cracks and large connected voids. Large voids that are not connected in the sample by these cracks remain unintruded. Figure 3B shows the intrusion process at 1000 psi in which the crack penetration is pronounced and large connected voids are filled. The extremely porous regions between closely spaced aggregate particles are also filled. Figure 3C shows the 1500-psi sample. The threshold diameter for this sample (according to MIP, see Fig. 5) occurs at a pressure between the 1000- and 1500-psi test pressures. Thus, a dramatic increase in the amount of intrusion between the two samples should be apparent. Also, by visual inspection, a noticeable darkening of the entire sample occurred after the threshold diameter was reached. In the 1500-psi sample, all the interfacial regions surrounding the aggregates are filled with metal and some of the groundmass has been intruded. The 3000-psi sample is shown in Figure 3D. In this sample, there is relatively uniform intrusion into the ground mass. The image shown for the 5000-psi sample (Fig. 3E) shows an intensification of this intrusion.

Early and late C-S-H

Figure 4 shows an unhydrated cement grain that has been highlighted during the intrusion process. The image clearly shows that the ground mass surrounding the grain has been fully infiltrated by the metal, whereas there seems to be a barrier surrounding the grain that will not allow further intrusion. This image elucidates the idea that the C-S-H formed in the early stages of hydration (which makes up the ground mass) is relatively porous compared to the C-S-H that is formed in the later stages of hydration (the C-S-H between the edge of the infiltrated ground mass and the unhydrated grain). As the image illustrates, at a pressure of 5000 psi, which corresponds to a pore diameter of about 0.03μm, this later C-S-H product has not been infiltrated.

Volume fraction and area analysis

In Figure 5, the pore volume fractions from Wood's metal samples (equivalent to area fraction calculated from the binary images) are compared to MIP results. The volume of

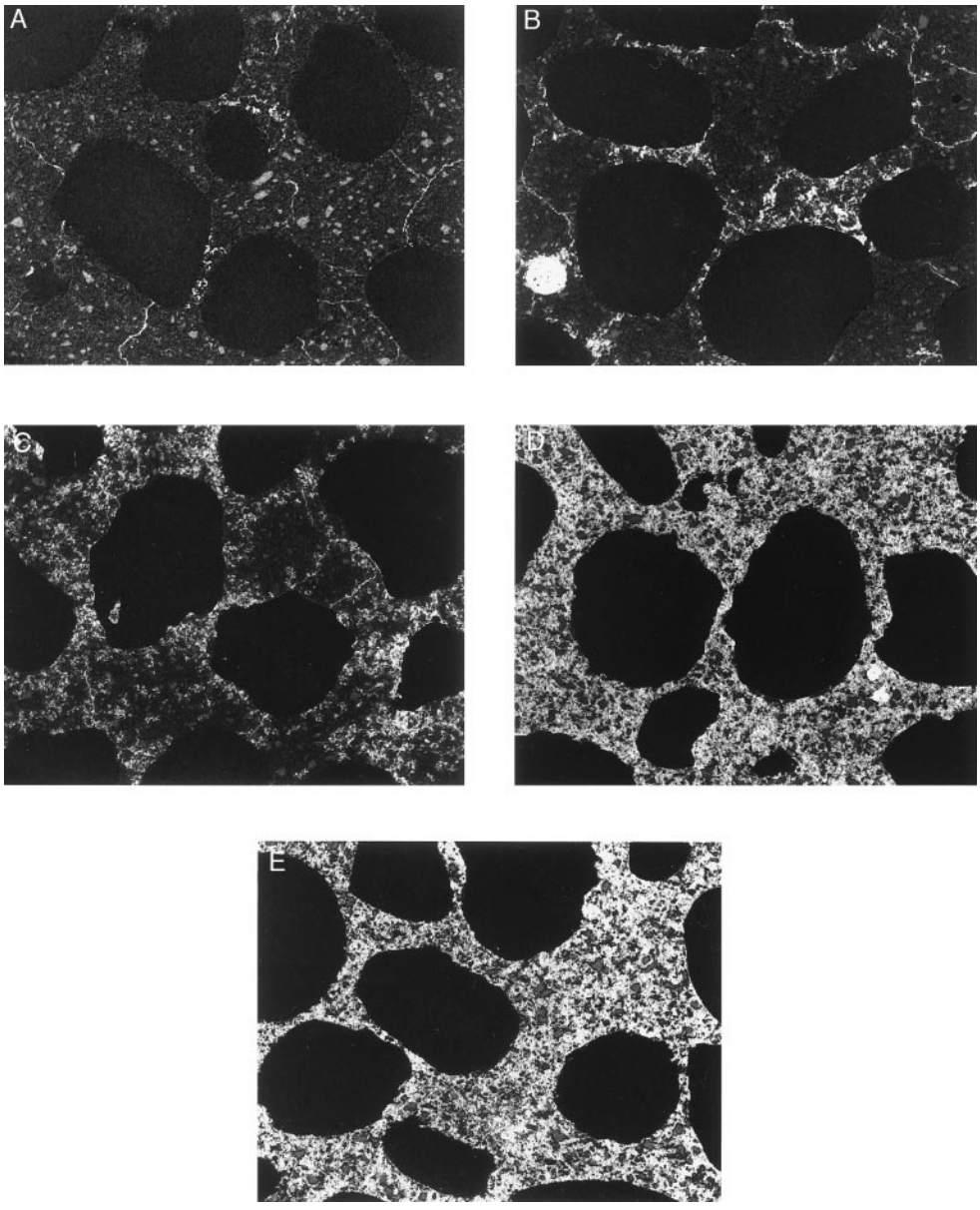

FIG. 3.
(*A–E*) A 0.6 w/c mortar showing sequence of intrusion (magnification 50×, field width 2.6 mm).

intruded mercury reported by MIP was converted to volume fraction by a calculation that used sample weight and specific gravity. There is excellent agreement between the volume of intruding mercury and the volume of molten Wood's metal that infiltrated the sample at each pressure. The threshold diameters agree quite well. With these results, confidence in the validity and reproducibility of the experiment was established.

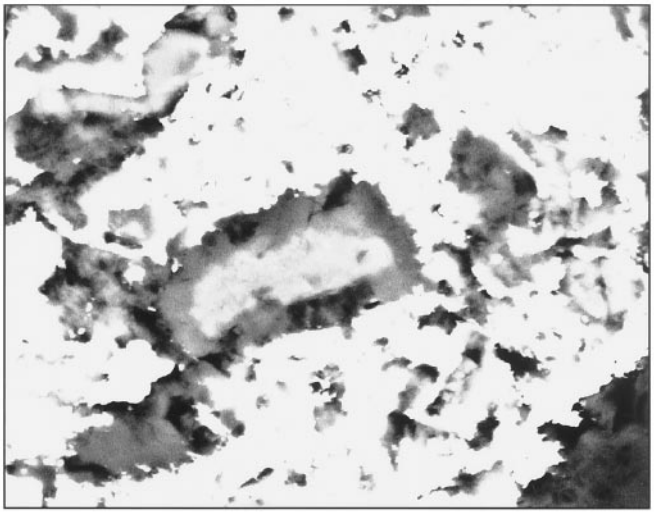

FIG. 4.
Unhydrated cement grain showing full intrusion of ground mass and no intrusion of C-S-H formed in later stages of hydration (magnification 1500×, field width 85 μm).

It can also be noted that the MIP curves show two distinct points at which the slope of the intrusion increases substantially (the intrusion curve for the 0.4 w/c sample demonstrates this more clearly). Whereas pastes usually have one drastic slope change at what is called the threshold diameter, this "two-humped" shape is common for mortars. When coupling the shape of this curve with the images in the intrusion sequence, insight into the types of features that are being intruded in each "hump" is gained. For the 0.4 w/c mortar, the first slope increase occurs at approximately 150 psi, which corresponds to a pore diameter of about 1.2 μm. Although a pressure as low as 150 psi was not tested by WMIP in this experiment, Figure 3A shows the condition of the microstructure after intrusion up to 500 psi. At 500 psi (pore diameter $\approx$ 0.36μm), only large cracks and voids have been intruded. Thus, at 150 psi it can be assumed that substantially less intrusion has occurred than is shown in this image. The second slope increase in the curve occurs at a pressure of about 1100 psi. From Figure 3C it is apparent that between the pressures of 1000 and 1500 psi the amount of intrusion within the microstructure of the sample increases dramatically. This implies that the majority of the intrusion in the first hump is occurring due to macrocracks and the seating of the nonwetting liquid into the rough texture of the exterior of the sample, whereas the second slope change is occurring when the threshold diameter of the microstructure is breached.

This idea is substantiated by the volume fraction comparison in Figure 5A. WMIP does not reveal the first hump of the MIP curve. However, the two curves do agree on the location of the second hump, which correlates to percolation of the pore structure. In the analysis of the Wood's metal micrographs, the edges of the samples were not considered. The intrusion in the first hump is attributed to the seating of the liquid in the texture of the sample and is not included in the Wood's metal results. This implies that the way in which a sample is prepared for MIP (whether it is crushed or saw cut) has an important effect on MIP results.

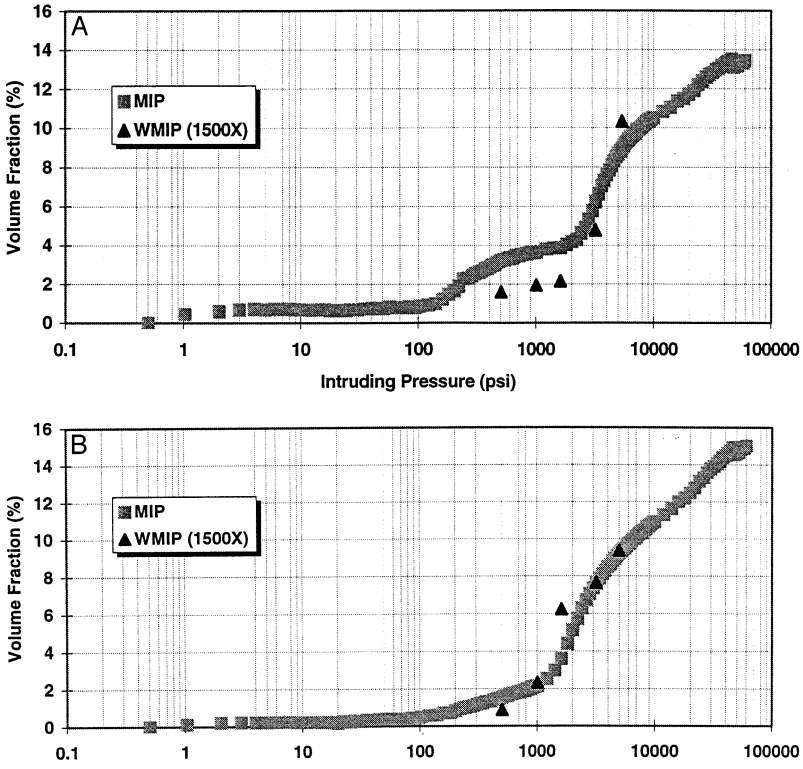

FIG. 5.
(*A*) Volume fraction analysis from 1500×, 15 keV images for the 0.4 w/c sample set. (*B*) Volume fraction analysis from 1500×, 15 keV images for the 0.6 w/c sample set.

Pore size analysis

The pore size (particle) distribution was analyzed using NIH Image by which the area and the major and minor axes of each pore were determined. The resulting cumulative intrusion and pore size distribution curves are shown in Figure 6. Images from the 5000- and 500-psi samples were evaluated to examine the shift in pores intruded as the pressure increases. Because the maximum intruding pressure used in the Wood's metal work was only 5000 psi, MIP data only up to 5000 psi (by the Washburn equation, this corresponds to a pore area of about 0.001 μm^2) were used.

The most important result of this study can be seen in Figure 6 in the comparison between MIP and Wood's metal. Figure 6 shows the results of the comparison between the cumulative intrusion curves for MIP at 5000 psi and WMIP at 5000 and 500 psi. The MIP curve shows much higher percentages of intrusion occurring at smaller pore sizes than that of the WMIP (5000 psi) curve. The limited intrusion observed in the 500-psi sample occurs at pore sizes between 1000 and 5000 μm^2, whereas the majority of the intrusion in the 5000-psi sample occurs between 0.01 and 30 μm^2. The MIP curve shows the largest volume of pores occurring below 0.01 μm^2. MIP misrepresents pore sizes because it measures pore size on the

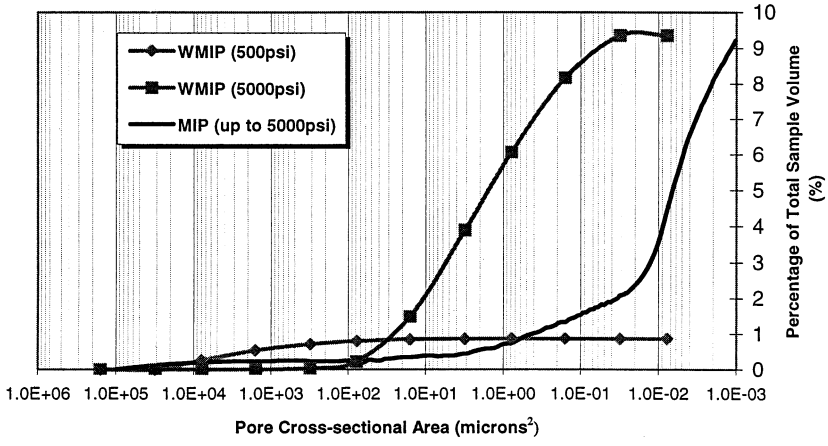

FIG. 6.
Cumulative intrusion curve for MIP and WMIP at 500 and 5000 psi (MIP data converted to areas using $A = \pi d^2/4$).

basis of diameter of access throat through which the mercury penetrates the microstructure to reach internal pores. This inherent error of MIP is called the "ink bottle effect." The ink bottle effect acts by assigning large pores the diameter of the smaller necks leading to them, and thereby skews the pore size distribution towards the smaller size range.

Conclusions

- A technique by which the principles of MIP are utilized to intrude molten Wood's metal into the pores of a sample where it solidifies has been developed.
- Two mortar samples of w/c ratios of 0.4 and 0.6 were intruded with molten Wood's metal at pressures ranging from 0–5000 psi. The samples were sectioned and observed in an SEM and analysis techniques were applied to the images.
- A qualitative, visual understanding of the way in which nonwetting liquids intrude a sample under pressure was obtained.
- The technique can differentiate regions of C-S-H formed later in hydration with a much finer porosity from those formed earlier in hydration.
- The volume of mercury intruded in each sample as obtained from MIP agrees well with the amount of Wood's metal intruded at each specific pressure as obtained from image analysis.
- A physical mechanism has been proposed to explain the smaller hump in the MIP curve that can occur at about 150 psi. MIP is sensitive to exterior texture and cracks in a sample and intruded volume at this low pressure is not related to capillary porosity.
- Pore size distribution curves are obtained and show that the size distributions obtained from MIP are shifted more towards smaller pores than those obtained from WMIP and image analysis.

Acknowledgments

This research was supported by the NSF Center for Advanced Cement-Based Materials (NSF Grant # DMR 88808423-01) and NSF Career Award (Grant # CMS-9623467).

References

1. T.C. Powers and T.L. Brownyard, J. Am. Concr. Inst. Proc. 43 (1946–1947).
2. E.W. Washburn, Proc. Natl. Acad. Sci. 7, 115 (1921).
3. D.N. Winslow, M.D. Cohen, D.P. Bentz, K.A. Snyder and E.J. Garboczi, Cem. Concr. Res. 24, 25 (1994).
4. J. Jambor, Influence of Water-Cement Ratio on the Structure and Strength of Hardened Cement Paste, Hydraulic Cement Pastes: Structure and Properties, Cement and Concrete Association, 1976.
5. D.J. Cook and H.T. Cao, An Investigation of the Pore Structure in Fly Ash/OPC Blends, Pore Structure and Construction Properties, Proceedings of the First International Congress, RILEM/AFREM, Vol. 1, pp. 69–76, 1987.
6. U. Schneider and U. Diedrichs, Detection of cracks by mercury penetration measurements. Fracture Mechanics of Concrete, S.P. Shah, S.E. Swartz and C. Ouyang (eds.), Wiley, New York, 1995.
7. P.K. Mehta and D. Manmohan, Pore Size Distribution and Permeability of Hardened Cement Pastes, Paris International Congress on the Chemistry of Cement, pp. VII 1–4.
8. R.J. Good and R.S. Mikhail, Powder Technol. 29, 53 (1980).
9. R.J. Good and J.K. Pascheck, Wetting, Spreading and Adhesion, F. Paddy (ed.), p. 147, Academic Press, New York, 1978.
10. R.F. Feldman, J. Am. Ceram. Soc. 67, 30 (1984).
11. R. Olson, C. Neubauer and H. Jennings, J. Am. Ceram. Soc. 80, 54 (1997).
12. F.A.L. Dullien, Powder Technol. 29, 109 (1981).
13. F.A.L. Dullien and G.K. Dhawan, J. Colloid Interface Sci. 52, 129 (1975)
14. K. Scrivener and K. Nemati, Cem. Concr. Res. 26, 35 (1996).
15. C. Chang, P. Monteiro, K. Nemati and K. Shyu, J. Mater. Civil Engng. 8, 157 (1996).
16. Metals Handbook: Properties and Selection: Nonferrous Alloys and Special Purpose Materials, Vol. 2, 10th ed, ASM International.